ELSEVIER

Journal of Photochemistry and Photobiology A: Chemistry 149 (2002) 175–181

Journal of Photochemistry and Photobiology A:Chemistry

www.elsevier.com/locate/jphotochem

Effect of improved crystallinity of titanium silicalite-2 on photodecomposition of simple aromatic hydrocarbons

Man Gu Kang, Han Seok Park, Kang-Jin Kim*

Division of Chemistry and Molecular Engineering, Korea University, 5-1 Anam-Dong, Seongbuk-Gu, Seoul 136-701, South Korea

Received 1 April 2001; received in revised form 15 August 2001; accepted 5 December 2001

Abstract

Time-dependent change in the concentrations of some aromatic hydrocarbons with TiO_2-based catalysts under irradiation was monitored by absorption spectroscopy. Titanium silicalite-2 with higher crystallinity (TS-2h) showed greater photodegradation efficiency than titanium silicalite-2 (TS-2). The greater efficiency was attributed to the increased adsorptivity based on the larger distribution coefficient arising from the more hydrophobic nature in the TS-2h cavity than in TS-2. The distribution coefficient correlates well with the slope of the Langmuir–Hinshelwood equation, and can be a useful index for the relative photodegradation efficiency of the aromatic hydrocarbon.

Keywords: Crystallinity; Photodecomposition; Aromatic hydrocarbons

1. Introduction

In recent years, the photocatalytic degradation of pollutants using semiconductors under ultraviolet irradiation has attracted considerable attention for application to environmental problems [1–8]. The photodegradation of pollutants is initiated by the attack of the photogenerated holes or subsequently produced hydroxyl radicals on the surface of semiconductor particles. Many studies [9–15] suggest that highly oxidizing hydroxyl radicals are produced in two ways: oxidation of hydroxide ions or water molecules adsorbed on the surface of semiconductor particles by photogenerated holes, and a series of redox reactions from trapping photogenerated electrons by oxygen.

To improve the photocatalytic efficiency for charge transfer from the catalysts to pollutants, the adsorption of pollutants on the photocatalysts has increased through the composite with SiO_2 [16–19], Al_2O_3 or zeolite [20–23]. Recombination of the photogenerated electron and hole is so rapid that interfacial charge transfer is kinetically competitive only when the pollutant is preadsorbed before photolysis. It has been suggested that preliminary adsorption is a prerequisite for the rapid efficient degradation of pollutants [24–29]. Many organic substrates can themselves act as adsorbed traps for the photogenerated hole, either directly or through the intermediacy of a surface hydroxyl radical [30–32]. Recent studies revealed that the photocatalytic activity toward the decomposition of phenol is improved with a mixed oxide of TiO_2/SiO_2 relative to TiO_2 [33,34]. The enhancement of the decomposition is attributed to the presence of a Ti–O–Si phase at the TiO_2/SiO_2 interface with the SiO_2 providing better adsorption sites in the vicinity of the TiO_2. Furthermore, titanium silicalites are reported to exhibit photocatalytic reactivities in the reduction of NO and aromatic pollutants with aqueous hydrogen peroxide [35,36]. A recent preliminary study on titanium silicalite-2 (TS-2) indicated a better photodegradation catalysis on 4-chlorophenol (4-CP) [37,38]. The nature of the environment of the cavity in TS-2 regarding its reactivity as a catalyst, however, needs to be further investigated.

This paper aims to improve the photocatalytic efficiency and to elucidate the relation between the photodecomposition rate of a pollutant in aqueous solution and its adsorptivity to a catalyst, based on a comparative investigation using TS-2, and TiO_2 (Degussa, P25). In particular, we were interested in the effect of increased crystallinity of TS-2 (hereafter TS-2h) on the photocatalytic efficiency with respect to TS-2. The irradiated solutions of simple aromatics were analyzed by UV absorption spectroscopy. The kinetics of the photodegradation on the catalysts was analyzed according to the Langmuir-Hinshelwood equation.

* Corresponding author. Tel.: +82-2-3290-3121; fax: +82-2-3290-3127.
E-mail address: kjkim@korea.ac.kr (K.-J. Kim).

1010-6030/02/$ – see front matter
PII: S1010-6030(01)00652-9

2. Experimental

2.1. Preparation for TS-2 and TS-2h

TS-2 was crystallized by the hydrolysis of tetraethylorthosilicate (TEOS) and tetrabutylorthotitanate (TBOT) using tetrabutylammonium hydroxide (TBAH) as a template [38,39]. 12.2 ml of TEOS was hydrolyzed in 14 ml of 40% TBAH aqueous solution under vigorous stirring for 30 min. To complete the hydrolysis, 0.55 g of TBOT in 5 ml of isopropyl alcohol was slowly added. The resulting gel was heated slowly at 80 °C and kept for 2 h under stirring followed by adding 19 ml of water, and then transferred into a 35 ml Teflon flask. The flask was placed in a static autoclave and crystallized at 175 °C for 24 h. The crystallized TS-2 was recovered by filtering, washed with water, and dried overnight in an oven at 110 °C. Finally, TS-2 was calcined at 500 °C for 5 h. TS-2 of a higher crystallinity (TS-2h) was prepared by the same procedure above, but using 6.1 ml of TEOS, 7 ml of 40% of TBAH, 0.27 g of TBOT in 2.5 ml of isopropyl alcohol, and 9.5 ml of water.

2.2. Characterization of TS-2 and TS-2h

X-ray powder diffraction patterns were obtained by using a Macscience M03XHF diffractometer at room temperature utilizing Ni-filtered Cu Kα radiation with 40 kV, 30 mA at 0.02° width and 4°/min scan speed. A Bomem, Hartman & Braun MB-series spectrometer utilizing KBr pellets was used to obtain IR spectra. UV reflectance spectra were recorded on a Varian CARY-5G spectrophotometer. Surface area was calculated using the BET equation from N_2 adsorption data at 77 K with a Micromeritics ASAP 2010 instrument. Atomic concentration was analyzed with a Perkin-Elmer OPTIMA 3000XL ICP spectrometer.

2.3. Distribution coefficients and oxidation potentials

The distribution coefficient (D) of an aromatic hydrocarbon (Aldrich) is obtained as the ratio of the amount on the catalyst, A_s, to that remaining in aqueous solution, A_a, after the equilibrium is reached

$$D = \frac{A_s}{A_a} \quad (1)$$

For the measurement of D, TS-2 or TS-2h powder was added into a flask containing an aqueous solution of 1.0×10^{-4} M of an aromatic hydrocarbon. The concentration of the powder was kept at 1 g/l. After stirring for 1 h, the powder was filtered at 3500 rpm with a Hanshin Medical HC-16A centrifuge followed by measuring the absorption spectrum of the resulting solution with a Hewlett Packard 8453 diode array spectrophotometer.

To obtain the oxidation potentials of the aromatic hydrocarbons, cyclic voltammograms were recorded with an EG&G Princeton Applied Research model 273 potentiostat at 50 mV/s using a Pt working electrode, a Pt counter electrode, and a Ag/AgCl reference electrode. The concentrations of the aromatics and $LiClO_4$ as electrolyte were 1.0×10^{-3} M and 0.5 M, respectively.

2.4. Photodegradation

A photochemical reactor was made of Pyrex glass with a plain quartz window and a water-circulating jacket. The reactor contained 50 ml of 1.0×10^{-4} M aromatic hydrocarbon solution and 1.0 g/l catalyst. Irradiation was carried out for 1 h through the quartz window with a 250 W xenon lamp (Ilctec) in air under stirring. After the irradiation, the catalyst was filtered and the absorption spectrum of the resulting solution was recorded.

3. Results and discussion

3.1. Basic characteristics

XRD, SEM, IR, and UV reflection characterized the catalysts. Fig. 1 compares the XRD spectra of a xerogel, TS-2, and TS-2h measured under the same condition. The xerogel was almost completely amorphous having no peaks related to TS-2. After crystallization, the characteristic peaks of TS-2 and TS-2h at $2\theta = 7.9°$, 8.8°, 23.2° and 24.0° were observed [39]. A comparison of the peak area under the peak at $2\theta = 7.9°$ indicates that the amount of the crystalline form in TS-2h was greater than in TS-2. Moreover, the peaks become sharper with increasing crystallinity, indicating crystal growth, which agrees with the SEM images contrasted in

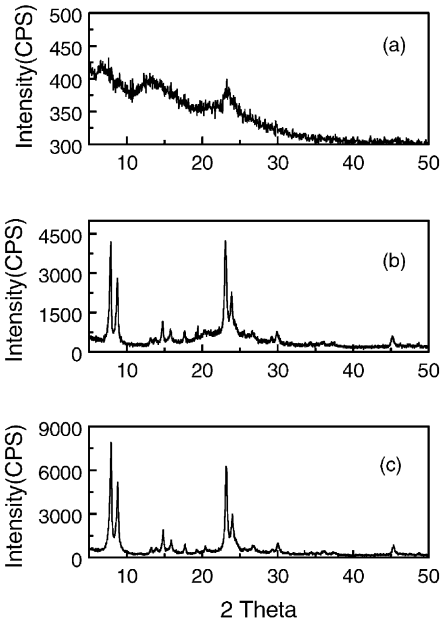

Fig. 1. XRD spectra of: (a) SiO_2–TiO_2 xerogel; (b) TS-2; (c) TS-2h.

(a)

(b)

Fig. 2. SEM images of: (a) TS-2; (b) TS-2h.

Fig. 2. TS-2h appears to form bundles of bigger crystallites, by ca. 30% on average, compared to TS-2. A variation of the amount of reactants reproducibly produces the same TS-2h, indicating that TS-2h possesses a stable crystallinity.

The IR spectra of both TS-2 and TS-2h showed a band at 960 cm^{-1}, which has been assigned to the stretching vibration of Si–O–Ti, arising from SiO_2 units linked to Ti atoms. The presence of the band suggests that Ti atoms have been effectively incorporated into the SiO_2 lattices [40]. From the UV reflectance spectra, absorption edges calculated by the Kubelka–Munk function were about 300 nm for TS-2 and TS-2h, and 380 nm for TiO_2. The blue shift of the absorption edge of TS-2 and TS-2h with respect to TiO_2 indicates that TiO_2 in both TS-2 and TS-2h is isolated with tetrahedral coordination. The Ti atomic concentration in TS-2 and TS-2h was found to be about 3% from an analysis by ICP spectrometry. The surface areas of TS-2h, TS-2 and Degussa P-25 TiO_2 were found to be 550, 360 and 58 m^2/g, respectively. Despite the larger crystal size of TS-2h, its higher degree of crystallinity creates more cavities within the crystal, generating a larger surface area than that of TS-2.

Table 1
Distribution coefficients (D) in TS-2, solubilities in water (g/100 g) and the logarithm of partition coefficients in octanol/H_2O ($\log P_{oct}$) of some aromatics

No.	Aromatic hydrocarbon	D	Solubility	$\log P_{oct}$
1	Phenol	0.21	6.7	1.46
2	*o*-Cresol	0.42	3.1[a]	1.95
3	*m*-Cresol	0.62	2.5[a]	1.96
4	*p*-Cresol	0.87	2.3[a]	1.94
5	2-Chlorophenol	0.49		2.15
6	3-Chlorophenol	0.60		2.50
7	4-Chlorophenol	1.02		2.39
8	2,4-Dichlorophenol	0.39		
9	3,4-Dichlorophenol	0.31		
10	*p*-Tolualdehyde	17.30		
11	4-Chlorobenzaldehyde	20.76		
12	4-Hydroxybenzaldehyde	0.65	1	
13	2,4-Dichlorobenzaldehyde	0.50		
14	Benzoic acid	1.42	0.29	1.87
15	*p*-Toluic acid	1.48	0.01	2.27
16	4-Chlorobenzoic acid	2.2	0.02	2.65
17	Salicylic acid	0.04	0.2	2.26
18	1,4-Benzoquinone	1.36		0.20
19	2-Chlorobenzoquinone	1.21		
20	Hydroquinone	0	7	0.59
21	Chlorohydroquinone	0.02		
22	4-Chlorocatechol	0.18		
23	1,2,4-Benzotriol	0.05		
24	Aniline	0.62	3.5	0.90
25	Benzylalcohol	0.98	0.08	1.10

[a] At 40 °C.

3.2. Distribution coefficients

To understand better the hydrophobic nature of the cavities of TS-2 and TS-2h, the distribution coefficient (D) was obtained according to Eq. (1). Table 1 lists the D values of TS-2 along with the data on solubility in water (g/100 g water) [41] and the logarithm of the partition coefficient, $\log P_{oct}$ [42,43]. P_{oct} is the partition coefficient for octanol–water system. We find the following list of substituents arranged in the order of decreasing the D: –CHO > –Cl > –COOH > $–CH_3$ > $–NH_2$ > –H > –OH. Among isomers with a –OH group, the D values decreases in the order: *para* > *meta* > *ortho*. Comparing 3-chlorophenol with 2,3-dichlorophenol and 3,4-dichlorophenol, although the D of the substituted aromatics with –Cl have been higher than that with –H, the D values decreases in the order: 3-chlorophenol > 2,3-dichlorophenol > 3,4-dichlorophenol. Also the D value of 2,4-dichlorobenzaldehyde decreases dramatically compared with 4-chlorobenzaldehyde. Thus, it appears that bulkiness of an aromatic hydrocarbon is important to the magnitude of D.

The D values apparently correlate well with the available solubility data (Fig. 3a) except salicylic acid. Since salicylic acid is a relatively strong acid, with $pK_a = 2.97$, more than

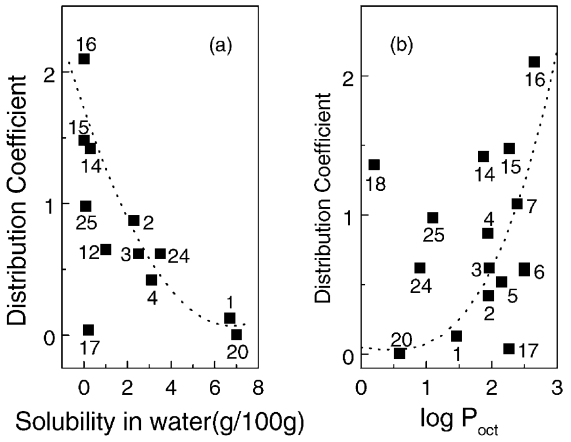

Fig. 3. Distribution coefficients vs. (a) solubilities in water and (b) partition coefficients in octanol–H_2O of various aromatic hydrocarbons.

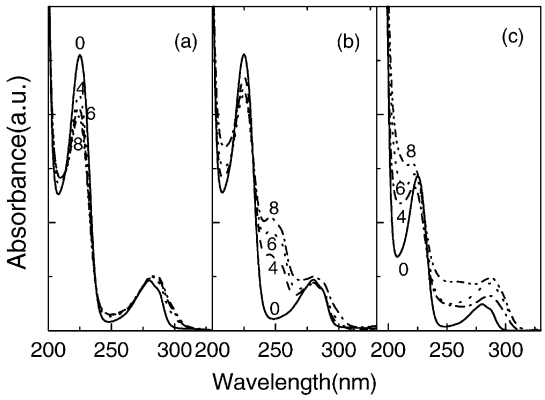

Fig. 4. Irradiation-time dependence of absorption spectra of 2.0×10^{-4} M 4-CP aqueous solution using: (a) TiO_2; (b) TS-2; (c) TS-2h catalysts in suspension. The numbers indicate the time of irradiation in minutes.

90% of the acid in 1.0×10^{-4} M solution exist as the deprotonated species. Assuming that the deprotonated species have limited access to TS-2, the *D* of the protonated form is calculated to be about 0.52, which is consistent with the general trend. A similar relationship is obtained with $\log P_{oct}$ (Fig. 3b). The deviations of aniline, benzyl alcohol, and benzoquinone (BQ) are noteworthy. Aniline appears to have a much lower $\log P_{oct}$, presumably because of forming an extra hydrogen bond. Benzyl alcohol apparently behaves like an aliphatic alcohol, which is more hydrophobic than an aromatic alcohol. Surprisingly, BQ has a very low $\log P_{oct}$, since the result implies that ethylenic carbon is actually hydrophilic. BQ appears to behave differently, since its electronic structure is different from the other aromatics. With a few exceptions, it may be concluded that the environment of the TS-2 cavity is hydrophobic. That is, the greater the hydrophobicity of the solute, the larger the *D*.

The TS-2h cavity is considered to be more hydrophobic than the TS-2 cavity, judging from the higher *D* values than TS-2 as shown in Table 2 for phenol (P), 2-chlorophenol (2-CP), 4-chlorophenol (4-CP), and 4-chlorobenzoic acid (4-CBA).

3.3. Photodegradation of 4-CP

In order to identify absorption peaks and to select appropriate wavelengths to monitor the reaction rate, absorption spectra of authentic aqueous solutions of the materials of interest were recorded. It is found that the broad absorption peaks appear at 225 and 280 nm for 4-CP, at 246 nm for BQ, at 221 and 290 nm for hydroquinone (HQ), and 221 and 284 nm for 4-chlorocatechol (4-CC). The last three compounds are known to be stable reaction intermediates produced from the photodecomposition of 4-CP [10]. However, a GC/MS analysis did not detect the presence of 4-CC under the present experimental condition [7].

Irradiation of solutions containing 4-CP in the presence of suspended TiO_2, TS-2 and TS-2h yielded time-dependent spectra as shown in Fig. 4a–c, respectively. Under dark condition, virtually no change in the concentration of 4-CP was detected. Fig. 5a constructed by the absorbance decrease at 225 nm shows that the 4-CP photodecomposition enhances in the presence of TS-2h, indicating that TS-2h is a better catalyst than TS-2.

Despite the lower surface TiO_2 concentration by about 19% and the larger band gap of the TS-2 catalyst relative to the TiO_2 catalyst, the photodecomposition rate is enhanced

Table 2
Data for distribution coefficient (*D*), apparent reaction rate constant (k_a) in 10^{-3} mol l^{-1} h^{-1}, and adsorption constant (*K*) in 10^3 l mol^{-1} on TS-2 and TS-2h

	TS-2				TS-2h			
	D	k_a	*K*	$k_a \times K$	*D*	k_a	*K*	$k_a \times K$
P	0.21	0.57	4.00	2.28	0.38	0.70	4.20	2.94
2-CP	0.49	0.60	4.25	2.55	0.86	0.80	4.13	3.55
4-CP	1.02	2.04	4.35	8.87	2.35	2.30	5.00	11.5
4-CBA	2.2	1.94	5.32	10.3	4.92	2.02	6.22	12.6

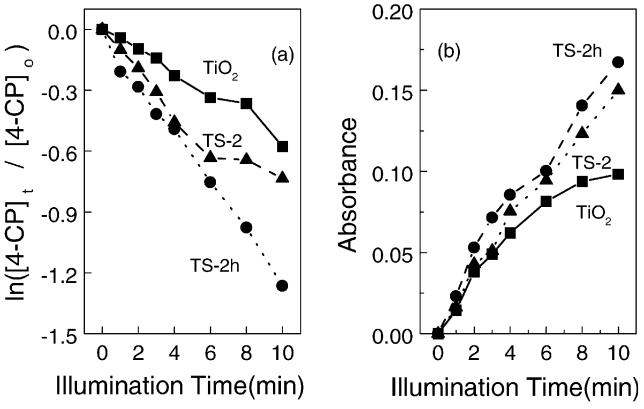

Fig. 5. (a) Irradiation-time dependence of the relative concentration of 4-CP at 225 nm; (b) time-courses of the absorbance of HQ at 300 nm of illuminated 4-CP aqueous solution using TiO_2, TS-2, and TS-2h catalysts in suspension.

with TS-2. The larger photoreactivity can be attributed to the increased adsorption of 4-CP due to the more hydrophobic environment of the TS-2 catalyst. From the *D* values, it is calculated that more than half of 4-CP is adsorbed on TS-2, whereas less than 1% of 4-CP is adsorbed on TiO_2. The increase in adsorption of 4-CP on TS-2 can cause an increase in efficiency of charge transfer from the photoinduced holes on TS-2 to 4-CP. A similar explanation can be applied to TS-2h. The photodecomposition rate with TS-2h compared with TS-2 is enhanced (Fig. 5a). It is found that 70% of 4-CP is adsorbed on TS-2h because of $D = 2.35$ (Table 2), and the surface TiO_2 concentration is increased by about 28% because of increasing surface area from 360 m^2/g for TS-2 to 550 m^2/g for TS-2h. Thus, the larger photoreactivity of TS-2h is also attributable to the stronger adsorption ability and the larger surface TiO_2 concentration due to the larger surface area in the TS-2h catalyst.

It is interesting to find that HQ hardly adsorbs to TS-2 and TS-2h whereas about 58% of BQ adsorbs to TS-2 (Table 1). This non-adsorptivity of HQ implies that HQ is excluded from the catalysts upon its formation. Therefore, [HQ] in solution can be indicative of the reaction as the decrease in [4-CP]. To confirm this notion, [HQ] was calculated using 1700 M^{-1} cm^{-1} as its molar absorptivity at 300 nm [7]. 4-CP, BQ and even 4-CC has almost no absorption at wavelengths longer than 300 nm. The result in Fig. 5b shows that the HQ concentrations produced in solution at 10 min are found to be 9.7×10^{-4}, 8.8×10^{-5} and 5.9×10^{-5} M for TS-2h, TS-2 and TiO_2, respectively, and correlate relatively well with Fig. 5a.

3.4. Comparison of photodegradation

To confirm that the photocatalytic reactivity is linked to the hydrophobicity of the catalyst, a comparison of the reactivity was made with phenol, 2-CP, 4-CP, and 4-CBA. The oxidation potentials of these aromatic hydrocarbons are calculated through the first derivative of the cyclic voltammograms and found to lie in the range 0.7–0.8 V vs. NHE. The differences in the oxidation potentials among the aromatic hydrocarbons are considered minute with respect to the energy difference between the photogenerated holes or hydroxyl radicals and the aromatic hydrocarbons. Thus, it is expected that the rates of charge transfer from the photogenerated holes to the aromatics do not differ very much. Fig. 6 clearly shows that there exist differences in the relative concentrations of the aromatics versus the irradiation time in the initial stage of the respective photochemical reactions. The differences in the relative concentration in the presence of the catalysts with respect to those in the absence of the respective catalysts are plotted in Fig. 7. From this result, the direct photodegradation of aromatics by UV light was subtracted from that on the catalysts, leaving only the contribution of the catalysts. The net photodegradation rates of the aromatics on the TS-2 and TS-2h catalysts respect to those in the absence of the corresponding catalysts decrease

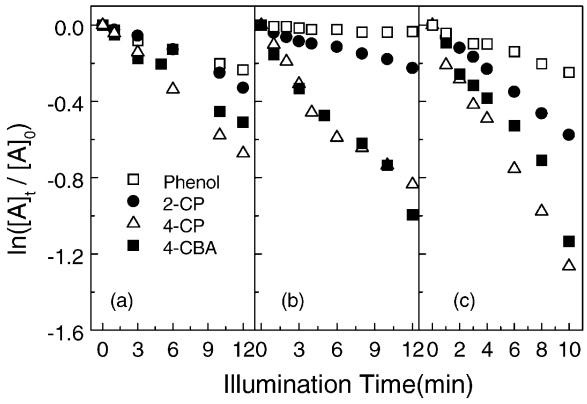

Fig. 6. Irradiation-time dependence of the relative concentration of the aromatics in aqueous solution with: (a) TiO_2; (b) TS-2; (c) TS-2h catalysts in suspension (concentrations: catalyst, 1 g/l; aromatics, 2×10^{-4} M).

in the order: 4-CBA > 4-CP > 2-CP > phenol. The result indeed demonstrates that the larger the *D*, the faster the initial reaction rate. Furthermore, the net photodegradation rates on TS-2h are faster than on TS-2. That is, an aromatic hydrocarbon having a stronger adsorption on a greater hydrophobic catalyst decays faster because of the increasing catalytic efficiency on the adsorbed aromatic hydrocarbon by the photogenerated holes.

The net photodegradation rate of 4-CBA on TiO_2, corrected for the direct contribution, is faster than the three phenols. This result can be explained by assuming that –COOH in 4-CBA can form a stronger bond with Ti–OH than –OH and –Cl in the phenols, increasing efficiency of charge transfer to 4-CBA by the photogenerated holes.

3.5. Kinetics of photodegradation

The effect of the crystallinity on the photodecomposition was compared under the same condition. It is expected that the reaction should follow an identical mechanism whether

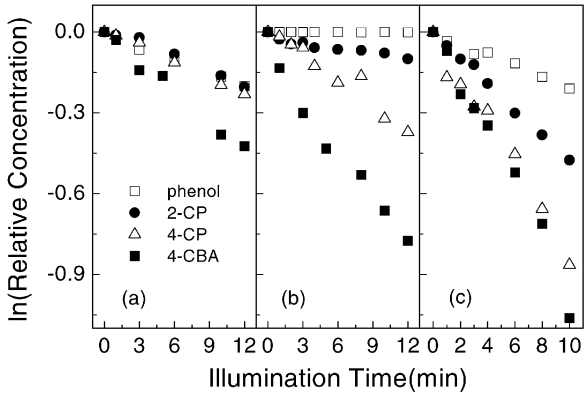

Fig. 7. Irradiation-time dependence of the relative concentration of the aromatics in aqueous solution with: (a) TiO_2; (b) TS-2; (c) TS-2h catalysts corrected for direct photodegradation by UV light (concentrations: catalyst, 1 g/l; aromatics, 2.0×10^{-4} M).

TS-2 or TS-2h was used. The photocatalytic degradation rate of 4-CP can be evaluated with apparent reaction rate constant, k_a, adsorption coefficient, K, and initial concentration of the pollutant, according to the inverse of the Langmuir–Hinshelwood equation.

$$-\frac{dt}{d[4\text{-CP}]} = \frac{1}{k_a} + \frac{1}{\{k_a K[4\text{-CP}]\}} \quad (2)$$

The k_a and K values derived from the intercept and slope are summarized in Table 2. The apparent reaction rate constants with TS-2h are found to be larger than with TS-2, confirming the qualitative results obtained above from the decreases in the absorbance of the irradiated pollutants with the time of irradiation. The K values can also be related to the D values of the pollutants. That is, the larger the D values, the larger the K values (Table 2). The values of K and D of pollutants on the TS-2h are larger than on TS-2.

In addition, the D correlates well with the product $k_a \times K$ and can be a useful index for the relative photodegradation efficiency of a pollutant on the catalyst. The order of the $k_a \times K$ values in Table 2 is consistent with the result that the order of the net photodegradation rate with TS-2h and TS-2 is 4-CBA > 4-CP > 2-CP > phenol (Fig. 7). Moreover, whereas the k_a of 4-CP was not greatly different from 4-CBA, the $k_a \times K$ value of 4-CBA was obtained to be distinctively larger than that of 4-CP. Thus, the values of $k_a \times K$ can reflect the photodegradation efficiency of the aromatic hydrocarbons with the catalysts.

4. Conclusion

We have conducted a comparative study on the time-dependent variation in some aromatic hydrocarbon concentration in the presence of TiO_2, TS-2 and TS-2h catalysts under irradiation. The photodecomposition rate can be attributed to the adsorptivity of the aromatic hydrocarbons onto the catalysts. TS-2h with higher crystallinity over TS-2 showed faster photodegradation rates than TS-2 due to the larger distribution coefficients of aromatic hydrocarbons onto the catalysts. The larger distribution coefficients on TS-2h arise from the greater hydrophobicity compared to TS-2. The distribution coefficient can be a useful index to reflect the photodegradation efficiency of the aromatic hydrocarbons on the catalyst.

Acknowledgements

This work was supported by the Center for Electro- and Photo-responsive Molecules.

References

[1] M.M. Hanmann, Photodegradation of Water Pollutants, CRC Press, New York, 1995.
[2] M.R. Hoffmann, S.T. Martin, W. Choi, D.W. Bahnemann, Chem. Rev. 95 (1995) 69.
[3] A. Mills, S.L. Hunte, J. Photochem. Photobiol. A 108 (1997) 1.
[4] R.A. Doong, W.H. Chang, J. Photochem. Photobiol. A 107 (1997) 239.
[5] K. Vinodgopal, U. Stafford, K. Gray, P.V. Kamat, J. Phys. Chem. 98 (1994) 6797.
[6] J. Theurich, M. Lindner, D.W. Bahnemann, Langmuir 12 (1996) 6368.
[7] M.G. Kang, H.E. Han, K.-J. Kim, J. Photochem. Photobiol. A 125 (1999) 119.
[8] X. Li, J.W. Cubbage, T.A. Tetzlaff, W.S. Jenks, J. Org. Chem. 64 (1999) 8509.
[9] V. Brezova, A. Stasko, S. Biskubic, A. Blazkova, B. Havlinova, J. Phys. Chem. 98 (1994) 8977.
[10] L. Zang, C.-Y. Liu, X.-M. Ren, J. Chem. Soc., Faraday Trans. 91 (1995) 917.
[11] J.M. Kesselman, O. Weres, N.S. Lewis, M.R. Hoffmann, J. Phys. Chem. B 101 (1997) 2637.
[12] Y. Ohko, K. Hashimoto, A. Fujishima, J. Phys. Chem. A 101 (1997) 8057.
[13] J.M. Kesselman, G.A. Shreve, M.R. Hoffmann, N.S. Lewis, J. Phys. Chem. 98 (1994) 13385.
[14] L. Cermenati, P. Pichat, C. Guillard, A. Albini, J. Phys. Chem. B 101 (1997) 2650.
[15] J. Schwitzgebel, J.G. Ekerdt, H. Gerisher, A. Heller, J. Phys. Chem. 99 (1995) 5633.
[16] C. Anderson, A.J. Bard, J. Phys. Chem. 99 (1995) 9882.
[17] N. Takeda, M. Ohtani, T. Torimoto, S. Kuwabata, H. Yoneyama, J. Phys. Chem. B 101 (1997) 2644.
[18] B.M. Reddy, I. Ganesh, E.P. Reddy, J. Phys. Chem. B 101 (1997) 1769.
[19] L.I. Alemany, M.A. Banares, E. Pardo, F. Martin, M. Galan-Fereres, J.M. Balsco, Appl. Catal. B 13 (1997) 289.
[20] X. Liu, K.-K. Lu, J.K. Thomas, J. Chem. Soc., Faraday Trans. 89 (1993) 1861.
[21] X. Yiming, C.H. Langford, J. Phys. Chem. 99 (1995) 11501.
[22] M. Anpo, H. Yamashita, Y. Ichihashi, Y. Fujii, M. Honda, J. Phys. Chem. B 101 (1997) 2632.
[23] H. Yamashita, Y. Ichihashi, M. Anpo, M. Hashimoto, C. Louis, M. Che, J. Phys. Chem. 100 (1996) 16042.
[24] T. Torimoto, S. Ito, S. Kuwabata, H. Yoneyama, Environ. Sci. Technol. 30 (1996) 1275.
[25] S. Tunesi, M. Anderson, J. Phys. Chem. 95 (1991) 3399.
[26] N. Takeda, M. Ohtani, T. Torimoto, S. Kuwabata, H. Yoneyama, J. Phys. Chem. B 101 (1997) 1769.
[27] N. Takeda, M. Ohtani, T. Torimoto, S. Kuwabata, H. Yoneyama, J. Phys. Chem. B 101 (1997) 2644.
[28] I. Ilisz, Z. Laszlo, A. Dombi, Appl. Catal. A 25 (1999) 180.
[29] J. Schwitzgebel, J.G. Ekerdt, F. Sunada, S.-E. Lindquist, A. Heller, J. Phys. Chem. B 101 (1997) 2621.
[30] Z. Liu, R.J. Davis, J. Phys. Chem. 98 (1994) 1253.
[31] F. Farges, G.E. Brown, A. Navrotsky, H. Gan, J.J. Rehr, Geochim. Cosmochim. Acta 60 (1996) 3039.
[32] M. Anpo, H. Nakaya, S. Kodama, Y. Kubokawa, K. Domen, T. Onishi, J. Phys. Chem. 90 (1986) 1633.
[33] M. Anpo, H. Yamashita, Y. Ichihashi, Y. Fujii, M. Honda, J. Phys. Chem. B 101 (1997) 2632.
[34] E. Karsen, K. Schoffel, Catal. Today 32 (1996) 107.
[35] V. Augugliaro, M. Schiavello, M. Palmisano, Corrdi. Chem. Rev. 125 (1993) 173.
[36] L. Palmisano, V. Augugliaro, R. Campostrini, M. Schiavello, J. Catal. 143 (1993) 149.
[37] M.G. Kang, J.S. Hong, K.-J. Kim, Chem. Lett. (1999) 885.
[38] M.G. Kang, H.S. Jung, K.-J. Kim, J. Photochem. Photobiol. A 136 (2000) 117.

[39] A. Thangaraj, R. Kumar, S.P. Mirajkar, P. Ratnasamy, J. Catal. 130 (1991) 129.
[40] M.A. Uguina, D.P. Serrano, G. Ovejero, R. VanGrieken, M. Camacho, Zeolites 18 (1997) 368.
[41] J.A. Dean, Lange's Handbook of Chemistry, McGraw-Hill, New York, 1992.
[42] A. Leo, C. Hansch, D. Elkins, Chem. Rev. 71 (1971) 525.
[43] A. Leo, Chem. Rev. 93 (1993) 1281.